Applied Energy 321 (2022) 119386

Contents lists available at ScienceDirect

Applied Energy

journal homepage: www.elsevier.com/locate/apenergy

Hard-coupling water and power system models increases the complementarity of renewable energy sources

Rachel Koh [a,*], Jordan Kern [b], Stefano Galelli [a]

[a] Pillar of Engineering Systems and Design, Singapore University of Technology and Design, Singapore 487372, Singapore
[b] Department of Forestry and Environmental Resources, North Carolina State University, Raleigh, NC 27607, United States of America

ARTICLE INFO

Keywords:
Water-energy nexus
Renewable energy
Hard-coupling
Hydropower
Power systems

ABSTRACT

The soft (one-way) coupling of water and power system models is the dominant approach for studying the impact of water availability on grid performance. Yet, such approach does not explicitly capture key dynamic interdependencies between the state of the grid and the operational decisions made at the water system level. Here, we address this gap and introduce a novel numerical modelling framework that hard-couples a multi-reservoir system model and a power system model. The framework captures two-way feedback mechanisms and thereby enables operational decisions to be made contingent upon the states of both the water and energy system. We evaluate the framework on a real-world case study based on the Cambodian grid. In light of the country's plan to further decarbonize its grid, we tested the framework on three grid configurations—the as-is grid, and the grid with two different levels of installed solar capacity. Simulation experiments were run with and without feedback, while uncertainty in external forcings was explored through 1,000 stochastic time series of streamflow, solar production, and load. As demonstrated in our results, hard-coupling the water and energy systems reduces operating costs and CO_2 emissions while increasing the integration of renewables. Under favourable conditions (large reservoir inflow and low electricity demand), the system experienced a 44% saving in annual operating costs and 53% reduction of CO_2 emissions. A spatio-temporal analysis on the reservoir operations and transmission line usage reveals that the timing of the monsoon and interconnections between individual grid components also play significant roles in influencing the system's responses to the hard coupling. Overall, simulation frameworks like this provide a modelling framework for testing management and planning solutions aimed to improve the performance of water-energy systems.

1. Introduction

Recognition of the interdependence between water and energy systems has motivated the research community to better understand the complex interactions within the water-energy nexus. Researchers often depend on numerical simulation models to represent these systems. Such models are particularly useful in evaluating potential system responses to important changes (e.g., integration of variable renewable energy into the grid) at both planning and operational stages. At the planning stage, longer-term simulations—usually employing monthly to annual time-steps over multi-decade horizons—facilitate the design of physical expansions of the grid or policies relevant to grid infrastructure [1–5]. In contrast, operational modelling of power grids involves simulation of system dynamics at the hourly to daily time-step (e.g., [6,7]). In this study, we focus on short-term operations of water-energy systems.

At the heart of the water-energy nexus, hydropower reservoirs play a paramount role. They fulfil multiple management objectives, including generating electricity for the power system, while being subject to varying hydro-meteorological conditions. The representation of hydropower reservoirs in numerical simulation models is therefore critical for a variety of applications. These applications include understanding the impact of droughts on power system performance [7,8] or supporting the integration of renewables [9]. Because reservoirs are a critical element of both water and energy systems, their study in a water-energy context typically builds on coupled models. This coupling process can be largely divided into two approaches: soft (one-way) and hard (two-way) [10]. Soft coupling approaches generally model the water and power systems separately, with information being fed unilaterally from one model to the other. For example, hydropower availability could be first simulated using a hydrological model [8,11]—or another ad hoc approach [7,12,13]—and then passed as a time series input to the power system model simulating the dispatch of electricity. While useful, softly coupled models can

* Corresponding author.
E-mail address: rachel_koh@mymail.sutd.edu.sg (R. Koh).

https://doi.org/10.1016/j.apenergy.2022.119386
Received 10 February 2022; Received in revised form 12 May 2022; Accepted 29 May 2022
Available online 9 June 2022

Nomenclature

Reservoir model

Q_d	Reservoir inflow on day d
$Q_{MAF,d}$	Mean annual flow for each calendar day
$Q_{MEF,d}$	Downstream environmental flow requirement on day d
R_d	Volume of water released through the turbines on day d
R_{max}	Maximum volume of water that can be turbined
S_{cap}	Capacity of the dam
S_d	Reservoir storage on day d
$spill_d$	Volume of water spilt from the reservoir on day d

Power system model

HP_d	Available hydropower on day d

Reservoir re-operation model

HP_t^{i*}	Hydropower dispatched from reservoir i in hour t
ϵ	Convergence limit
n	Maximum number of iterations to reach convergence

Stochastic inputs

HP_d	Available hydropower on day d
I_d^l	Irradiance "losses" on day d
I_{cs}^n	"clear sky' irradiance on calendar day n
I_{obs}^d	Observed irradiance on day d
$\widehat{I_d^l}$	Standardized irradiance loss on day d
$\mu(I_n^l)$	Average of I_d^l on calendar day n
$\sigma(I_n^l)$	Standard deviation of I_d^l on calendar day n
d_m^{obs}	Observed peak demand in month m
d_m^{pred}	Predicted peak demand in month m
D_m	Difference between the observed and fitted peak demand in month m
$t_{min,d}$	Daily observed minimum temperature
$\bar{t}_{min,m}$	Mean of the daily minimum temperature in month m
$\hat{t}_{min,d}$	Standardized temperature on day d
$\hat{D}_m$	Residual between the predicted and actual peak demand in month m
$\mu(t_{min,n})$	Mean of daily observed minimum temperature on calendar day n
$\sigma(t_{min,n})$	Standard deviation of daily observed minimum temperature on calendar day n

fail to capture complexities and nuances of water-energy systems. In particular, operating the water system components based only upon the hydrology and reservoir operating rules may erroneously assume that reservoir operators do not factor-in the state of the power system when making operational decisions. Yet, because of its limited complexity, the soft-coupling approach is, by far, the dominant approach used in research. Indeed, there are only a handful of studies that attempt to fully integrate two models—thereby capturing the feedbacks between one system to the other. For example, Ibanez et al. [14] hard-coupled RiverWare (a river routing model) with PLEXOS (a grid operations model) by iteratively optimizing the power system production costs while fulfilling the constraints of the water system. The application on the Western US showed favourable results in terms of production costs and curtailment of renewables. Recently, Stevanato et al. [15] demonstrated the importance of considering hydrological constraints on hydropower by integrating a reservoir model into Calliope, an energy modelling framework applied on the Zambezi River Basin in South Africa. Studying the possibility of storing hydropower when wind is available, Gebretsadik et al. [16] integrated an ad hoc reservoir system model with a single-node power system model and showed reduced reliance on thermal resources as a result.

Despite these recent studies, the full range of benefits from capturing these feedbacks is still poorly understood. Previous studies have focused exclusively on the generation mix as a key performance metric, but there are other benefits that have not been quantified yet. For example, transmission congestion can strongly affect the feasibility and value of hydropower production [17,18]. Enabling reservoir operational decisions to be contingent upon the states of both water and energy systems could help address this problem. Another important potential benefit is increasing the penetration of renewables, particularly wind and solar: given the intermittent nature of solar and wind generation, operationally flexible hydropower can be an complementary grid asset [19]. Hydropower reservoirs allow for storing and releasing water (and, therefore, potential energy) to buffer the variability of solar and wind. In addition, the benefits of hard-coupling water and energy models have until now been evaluated under deterministic conditions. Yet, it is widely known that uncertainties in load and variable renewable energy production can profoundly affect power system operations. It is thus important to incorporate these uncertainties in the further development and implementation of hard-coupled models. Furthermore, most grid representations in previous studies tend to be overly simple, which also limits our understanding of the importance of capturing feedbacks in water-energy systems models. For example, by modelling the electricity demand and supply of an entire region as a single-node, the role of important grid elements such as substations and transmission lines is not considered in the operational framework. Finally, we need to understand how the operations of non-hydropower grid components is affected by the representation of feedback mechanisms.

In this study, we contribute a novel numerical modelling framework for hard coupling water system and power system models. As highlighted in [20], grids with different kinds of renewable resources present multiple challenges, including spatial and temporal variability. For instance, reservoir releases that are made concurrently with high solar or wind generation may cause temporary "oversupply" of electricity, leading to forced curtailment or grid congestion issues [18]. To account for the effects of such external conditions, we introduce a reservoir re-operation model in our framework, a key element which gathers information from both the water and power systems. Specifically, the timing and amount of hydropower dispatched into the grid is compared to what is available to update water release decisions from hydropower reservoirs. This in turn allows the models more flexibility in responding to changes in external conditions. As we shall see, another important feature of the re-operation model is its capability to handle both single and multi-reservoir systems, thereby making it suitable for complex reservoir networks. Using a detailed representation of the Cambodian water-energy system, we demonstrate that the flexibility built into hard-coupled models can be exploited to improve the system's performance, measured in terms of operating costs, CO_2 emissions, and penetration of renewables. We also explore how uncertainty in external conditions (i.e., inflow, load, and solar power production) influences the benefits derived from this hard coupling. Finally, we zoom into finer spatio-temporal scales and investigate how specific grid behaviours are modified by the use of a re-operation model.

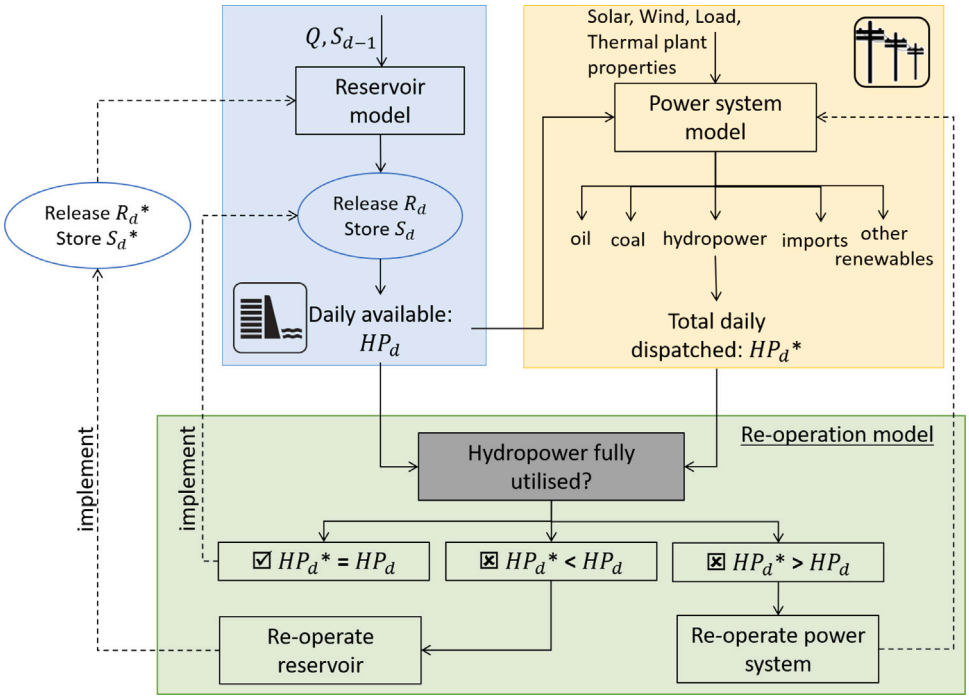

Fig. 1. Modelling framework, comprising a reservoir model, power system model, and re-operation model. The dashed lines represent the feedback from the re-operation model to the two primary models. Symbols are introduced in Sections 2.2, 2.3, and 2.4.

2. Methods

2.1. Overview

We now provide an overview of our approach for creating a hard integration of water and energy models. Our integrated model is written in Python and consists of: (1) a reservoir system model; (2) a power system model; and (3) a re-operation model (blue, yellow and green box, respectively, in Fig. 1). Note that in state-of-the-art multi-sector models, it is typical to find only two components, i.e., a reservoir model and a power system model with a one-way transfer of information (usually hydropower availability) from the former to the latter (e.g., [8,11,21]). The added re-operation component enables the hard integration of the two models, allowing for a two-way feedback between them. The re-operation component evaluates the outcomes of the decisions made by the two primary models and provides a feedback (see dashed line leading back) to the respective models. Details of the reservoir, power system, and re-operation models are provided in Sections 2.2, 2.3, and 2.4, respectively.

2.2. Reservoir system model

Hydropower reservoir operations depend on several factors, including the network topography, hydro-meteorological processes, and site-specific operating objectives. Many models have been developed to simulate the behaviour of such reservoir networks (e.g., [22–25]). Although they come with different assumptions and require different inputs, in general, these models accomplish several things: they (1) route water through the river network; (2) solve the mass balance in each reservoir; and (3) calculate the amount of hydropower available to be produced by each dam. Driven by the need to create a two-way integration with a power system model, we have initially chosen to demonstrate the value of our framework using an ad hoc reservoir model—which could be replaced in the future with any other river routing-water management model.

Key to our model is the representation of storage dynamics and hydropower availability in a reservoir network. For an headwater dam, the storage dynamics are described by the following daily mass balance:

$$\begin{aligned} S_d &= S_{d-1} + Q_d - R_d - spill_d, \\ 0 &\le S_d \le S_{cap}, \\ Q_{MEF,d} &\le R_d \le R_{max}, \end{aligned} \tag{1}$$

where S_d is the reservoir storage, Q_d the reservoir inflow, R_d the volume of water released through the turbines, $spill_d$ the volume of water spilt from the reservoir on day d, S_{cap} the capacity of the dam, $Q_{MEF,d}$ the downstream environmental flow requirement (described later), and R_{max} the maximum volume of water that can be turbined, representing the designed discharge capacity of the dam.

If the reservoir is located downstream of one or multiple reservoirs, the mass balance is modified to consider the natural inflow Q_d as well as the turbined and spilt water from the upper reservoir(s) (R_d^{upper}, $spill_d^{upper}$):

$$\begin{aligned} S_d &= S_{d-1} + Q_d - R_d - spill_d + R_d^{upper} + spill_d^{upper}, \\ 0 &\le S_d \le S_{cap}, \\ Q_{MEF,d} &\le R_d \le R_{max}. \end{aligned} \tag{2}$$

The decision variable for each reservoir within the network is R_d. This variable affects the operations of the reservoir and also influences the power system operations, since it determines the amount of hydropower available to the grid on a daily basis. To calculate initial values of R_d, we use rule curves, a common approach adopted by reservoir operators [8,26]. Simply put, a rule curve represents the target storage (or level) that a reservoir should maintain on each calendar day. Following Dang et al. [24], we define the rule curves as piece-wise linear functions based on four parameters (Fig. 2): the minimum and maximum water levels that a reservoir should reach within a year (H_1 and H_2) and the time at which the two levels should be reached (T_1 and T_2). For a given water system, these parameters can be reported by local agencies, retrieved from water storage data, or even inferred from satellite data [27]. The daily release decisions R_d from each reservoir are made to bring the actual storage as close to the target storage as possible, while being subjected to an upper

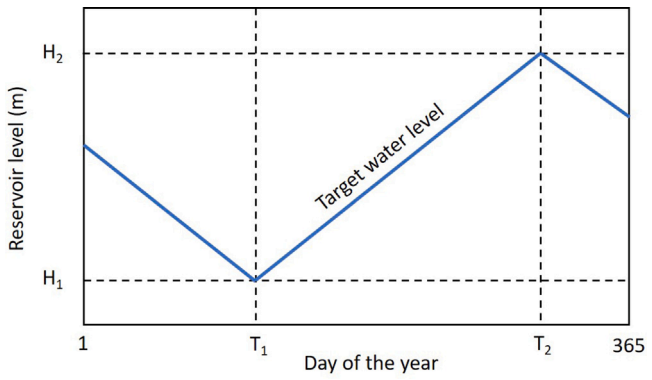

Fig. 2. A typical rule curve used for reservoir operations in our study. H_1 and H_2 are the minimum and maximum water levels that a reservoir should reach within a year, and T_1 and T_2 denote the time at which the two levels should be reached. The target water level is derived from a piecewise linear function based on the four parameters.

and lower bound (R_{max} and $Q_{MEF,d}$, respectively), as shown in Eq. (1) (see Section 1 in the SI for additional details about the rule curves). Following the method used in [28], the daily $Q_{MEF,d}$ are determined according to Eq. (3), where the daily reservoir inflows Q_d are classified as low, medium, and high compared to $Q_{MAF,d}$, the mean annual flow for each calendar day:

$$Q_{MEF,d} = \begin{cases} 0.6 \cdot Q_d & \text{if } Q_d \le 0.4 \cdot Q_{MAF,d} \text{ (low)} \\ 0.3 \cdot Q_d & \text{if } Q_d > 0.8 \cdot Q_{MAF,d} \text{ (high)} \\ 0.45 \cdot Q_d & \text{otherwise (medium)} \end{cases} \quad (3)$$

Finally, the daily available hydropower is calculated as follows:

$$HP_d = \eta \times \rho \times g \times R_d \times (H_{d-1} + H_d)/2, \quad (4)$$

where HP_d is the available hydropower (MW) on day d, η the turbine efficiency, ρ the water density (1000 kg/m^3), g the gravitational acceleration (9.81 m/s^2), and H_d the hydraulic head, taken as the average between days $d-1$ and d. To ensure that the storage dynamics do not deviate excessively from the rule curves, a verification of the reservoir operations model can be found in Figure S2 in the SI.

In softly-coupled models, the one-way flow of information involves the amount of available hydropower (HP_d) being communicated from the reservoir model to the power system model (refer to Fig. 1). This is usually done at the beginning of each day to set the upper bound for hydropower allocation in the power system model. Yet, there is no guarantee that the full hydropower allocation is needed by the grid; it could instead contribute to temporary oversupply, leading to HP_d not being fully dispatched. The goal of our hard-coupled framework is to tighten the coordination of water-power systems, thereby reducing the curtailment of renewable energy caused by excess of supply. On days when the full hydropower allocation is not needed by the grid, there may be benefits in re-operating the reservoir network (releasing less water and therefore producing less hydropower). The actual operations of the network will thus only be decided after gathering a feedback from the power system model.

2.3. Power system model

Multiple models have been developed to simulate the dynamics of large-scale power systems [14,21,29]. Here, we use PowNet [12], a highly customizable production-cost model that has been applied to Cambodia [12] and the Greater Mekong [8] for studying the vulnerability of the grid to hydro-climatic variability. PowNet solves a mixed integer linear program with the objective of meeting dynamic electricity demand at all substations at minimum cost. The decisions made by PowNet include (1) which generating units to start-up and shut down (unit commitment) and (2) the amount of power supplied by each unit (economic dispatch). The objective function of the model thus comprises operating costs, start-up costs, fuel prices and variable costs for the domestic thermal units, as well as import costs for the import nodes. The operations are also subjected to multiple constraints, such as ramping limits of the thermal plants, energy balance at each node, and capacities of the transmission lines. Importantly, modelling the power flow through the grid can provide insights into potential transmission congestion problems—such as those that may arise when incorporating increasing intermittent supply from renewables [17,18]. In contrast to the reservoir model, PowNet works at the hourly time step and with a planning horizon of 24 h. For each simulated day, PowNet outputs include hourly time series of operating costs, CO_2 emissions, and generation mix.

The model inputs include the parameters of the transmission lines (e.g., susceptance, capacity), the hourly time series of electricity demand at each sub-station, the parameters of the dispatchable units (e.g., capacity, O&M costs), and the hourly time series of power availability for renewable resources. The daily generation mixes of systems with a large percentage of renewables can fluctuate significantly due to the influence of seasonality and anomalies in hydro-meteorological processes. Unlike thermal plants—where operations are constrained by the plant specifications—the dispatch of electricity from renewable sources is limited by the availability of the resource. For non-dispatchables like solar and wind, the input to PowNet are the hourly time series of availability over 24 h, while for hydropower the input is the available hydropower (HP_d) calculated by the reservoir system model (Section 2.2).

2.4. Re-operation model

The reservoir and power system models have independent operating guidelines, so an additional model component is required to coordinate the two-way transfer of information between the two models [30]. The re-operation model (Fig. 1) orchestrates this exchange of information in our framework, including translating variables (i.e., available and dispatched hydropower, and reservoir release) between the two models by (dis)aggregating them to a finer or coarser resolution as necessary. The final goal of the re-operation model is to implement a 'globally optimal' reservoir operation strategy that accounts for the overall state of the water-energy system, using information from both reservoir and power models on a day-to-day basis. Importantly, the re-operation modelling framework can be applied to hydropower reservoirs in both individual and cascade configurations. In our explanation, we will first describe how the model works for single reservoirs, and then highlight the modifications required for cascade systems.

The re-operation model works in two steps:

Step 1: Compare and re-operate. On each day, the model compares the quantity of available hydropower HP_d^i simulated by the reservoir model with the quantity of hydropower dispatched by the power system model over 24 h for each reservoir i, HP_t^{i*}, where $t = 1, 2, \ldots, 24$ (from PowNet). This yields one of three outcomes, as detailed below. Depending on the outcome, the model decides whether or not to re-operate the reservoir and power system. At this point, it is important to note that the inflow to a reservoir with at least one other dam upstream will be altered if its upper reservoir has been re-operated to release less water. When evaluating such reservoirs, we have to update the mass balance (using Eq. (2)) based on the new inflow and derive the new hydropower availability HP_d^i (using Eq. (4)) before comparing it against the output of the power system model.

Outcome 1: $\sum HP_t^{i*} = HP_d^i$. All daily, available hydropower in reservoir i is fully dispatched. This is the simplest outcome. No re-operation is required in this case, and the final strategy for reservoir i is to release R_d^i according to the rule curve (Fig. 2).

Outcome 2: $\sum HP_t^{i*} < HP_d^i$. The available hydropower in reservoir i is not fully dispatched by the power system model. This triggers the re-operation of reservoir i, with the goal of generating only $\sum HP_t^{i*}$. In turn, this translates into a smaller release and more water storage available for future use. The re-operation steps are summarized in Algorithm 1. The main equations involved are the mass balance equation (Eq. (1)) and hydropower equation (Eq. (4)), so as to ensure consistency between the reservoir and power system operations. In Algorithm 1, we begin by substituting HP_d in Eq. (4) with $\sum HP_t^{i*}$, as this is the resulting hydropower that we would like to generate. Since all parameters from the previous time step $(d-1)$ are known, the only unknowns in this equation are R_d and H_d. To solve the equation, we first assume that the water level remains unchanged from the previous day, i.e. $H_d = H_{d-1}$. The next steps involve iteratively solving Eqs. (1)–(4) until the difference in the values of the release r obtained in two consecutive iterations are within the defined convergence limit ϵ, where ϵ is a small arbitrary constant. In sum, we proceed as follows:

(a) Calculate r from Eq. (4).
(b) Compare the obtained r against Q_{MEF}, d (derived from Eq. (3)) and adjust it accordingly if it does not fulfil the minimum flow requirements.
(c) Calculate $spill$ using Eq. (1).
(d) With the estimated r and $spill$, find the reservoir storage S using Eq. (1). If the reservoir has inflow from other reservoirs, Eq. (2) is used instead.
(e) Update the hydraulic head H_d with the derived reservoir storage S.

Algorithm 1 Reservoir re-operation algorithm (for Outcome 2)

Input:
$HP_t^{i*}\ \forall t = 1, ..., 24$
S_{d-1}^i, Q_d^i
ϵ, n
Output: R_d^{i*}, S_d^{i*}, $spill_d^{i*}$
Initialize: $H_k = H_{d-1}$
repeat
$r_k = \sum_{t=1}^{24} HP_t^{i*}/(\eta \times \rho \times g \times (H_{d-1} + H_k)/2)$ ▷ Eq. (4)
$r_k = \max(r_k, Q_{MEF,d})$
$spill_k = S_{d-1} + Q_d - r_k - S_{cap}$ ▷ Eq. (1)
$S_k = S_{d-1} + Q_d - r_k - spill_k$ ▷ Eq. (1) or Eq. (2)
$H_k \leftarrow S_k$ ▷ Update hydraulic head
$k = k + 1$
until $r_{k+1} - r_k \le \epsilon$ or $k + 1 \ge n$ ▷ Convergence
return $R_d^{i*} = r_k$, $S_d^{i*} = S_k$, $spill_d^{i*} = spill_k$

When r converges—or we have reached the pre-defined maximum number of iterations n—we complete the re-operation for reservoir i on day d and update the new state of the reservoir accordingly (release, storage, and spill on day d). The best strategy is thus for reservoir i to release $R_d^{i*} = r$.

Outcome 3: $\sum HP_t^{i*} > HP_d^i$. The dispatched hydropower in reservoir i exceeds the availability. Typical operations will not result in this outcome as the hydropower allocation in PowNet is bounded by HP_d^i. This outcome is thus unique to downstream reservoirs with inflow from other reservoir(s) when both of the following conditions occur: (1) at least one of the upstream reservoirs is re-operated (and thus releases less water), and (2) this reduction in inflow is significant enough to generate less hydropower than the power system model allocated from reservoir i. This makes the operation infeasible, and a feedback will be sent to PowNet to re-allocate its resources for day d based on an updated hydropower availability of reservoir i (HP_d^i). Once we obtain a new generation mix from PowNet, we re-evaluate the performance of all reservoirs again, i.e., repeat Step 1 for day d again.

Step 2: Implement best release strategy. The best release strategy based on the current system states is conveyed back to the reservoir model for implementation. This concludes the system operations for day d and the simulation will advance to the next day.

At the end of the simulation, we expect to achieve a better performance of the coupled system through more operationally flexible and informed use of the reservoirs—leading, for example, to lower system costs or better penetration of renewables. However, one natural consequence of re-operating the reservoirs is some deviation from the target storage levels recommended by the rule curves. As we shall see, strategic re-operation of reservoirs often involves (temporarily) storing more and releasing less water. As a result, more spills may be observed during wet seasons if the demand for hydropower is less than what is available. This is equivalent in some respects to curtailing wind and solar during periods of over-supply. To address such a matter, one could modify the re-operation model to explicitly account for other operating factors, such as hydropeaking, by tracking for example the day-to-day release decisions. However, these modifications are left as future explorations, because our chief objective is to identify the largest operational space (and corresponding benefits) associated with a tighter integration of water and energy systems.

3. Design of experiments

3.1. Case study

The modelling framework is tested on the Cambodian water-energy system, illustrated in Fig. 3. Specifically, our model implementation is based on the infrastructure built and operated in 2016, for which detailed data are available [12]. Domestically, the electricity demand is fulfilled by three coal-fired units (totalling 400 MW of installed capacity), 15 oil-fired units (totalling 282 MW), and six hydropower plants (totalling 1048 MW). Near the borders, Cambodia can import hydropower from Laos and thermal power from Vietnam (200 MW) and Thailand (120 MW). The domestic hydropower availability in Cambodia is largely influenced by the seasonality of the hydro-climate. Driven by the summer Monsoon, reservoirs tend to receive more inflow and generate more hydropower during the period spanning from May to October. The dam specifications are shown in Table 1. Note that Atay and LR Chrum are operated in cascade, while the rest are headwater dams.

The power system network features generators and substations connected by high-voltage transmission lines. The input data to PowNet, including the parameters of the dispatchable units and transmission lines, were extracted from technical reports [32,33]. The time series of electricity demand were also derived using information from the same reports, including the monthly peak national demand, and hourly

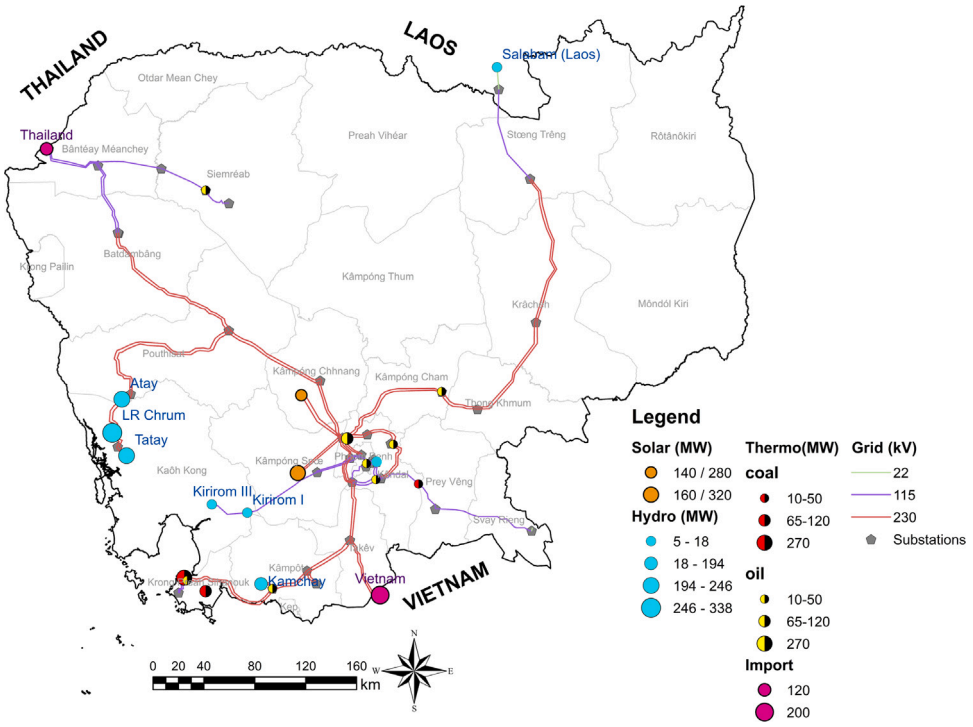

Fig. 3. Main generation and transmission components of the Cambodian power system, as of 2016. The location of the solar plants is based on the information provided by EDC [31], with arbitrary installed capacity. Further details are provided in Section 3.3.

Table 1
Design specifications of the Cambodian hydropower dams [32].

Name	Installed capacity (MW)	Dam height (m)	Storage (Mm^3)	Design discharge (m^3/s)	Hydraulic head (m)	Basin area (km^2)
Kamchay	194.1	110	680	163.5	122	710
Kirirom I	12	34	30	20	373.5	99
Kirirom III	18	40	30	40	271	105
Atay	240	45	443.8	125	216	1157
LR Chrum	338	68	62	300	132	1550
Tatay	246	77	322	150	188	1073

demand profiles for weekdays and weekends. To get the hourly load for each substation, we relied on a spatial and temporal disaggregation of the national data. In particular, we first interpolated between the monthly peak demand data to obtain the daily peak national demand, and then disaggregated it further using weekday-weekend and peak-off-peak demand profiles to account for the variation among days in a week and hours in a day. As for the spatial disaggregation, we dispersed the national demand to the substations based on their voltage levels to yield the hourly load at each substation. We note that the electricity demand time series so derived do not show day-to-day changes in demand due to weather; however, they implicitly capture the seasonal sensitivity to air temperatures—a driver of air conditioning need—which slightly increases in pre-monsoon months. At the substation with the highest demand, we added a hypothetical "slack" generator with arbitrarily assigned parameters and very high production cost to prevent electricity shortage [12]. Further details about the model setup and validation are reported in [12].

3.2. Stochastic inputs

To characterize the benefits of co-simulating the water and energy systems, we conduct a probabilistic assessment of the system performance by generating stochastic replicates of the input variables. Since the water-energy system is susceptible to both hydrological and meteorological uncertainty, the inputs required in our set-up include streamflow (for the reservoir model), and electricity demand and solar power production (for the power system model). In particular, each variable is synthetically expanded to produce 1000 single-year time series. A random combination of the expanded time series will allow us to have a better understanding of how the system performance evolves with different inputs as they form potential scenarios that drive the system's responses. In the stochastic generation process, we assume that the three processes are independent—an assumption that was verified through the observational historical datasets.

3.2.1. Streamflow

It is especially important to explore the variability in streamflow as Cambodia is subjected to pronounced hydro-climatic variability due to the summer monsoon (Section 3.1). The stochastic model that we require should therefore be able to capture the monsoonal effects in the generated streamflow while ensuring that the spatial correlation of the inflow across the six reservoirs is well represented. The Kirsch–Nowak Streamflow Generator fulfils the required features, with a stochastic model that produces correlated synthetic daily streamflow time series at multiple sites [34]. Besides the generator engine, the model also consists of a monsoonal rescaling function to capture inter-annual variability in the monsoon [35]. This stochastic model has been used to generate synthetic streamflow in other regions of Southeast Asia, such as Vietnam [36,37].

Daily inflow data for the six reservoirs in our study were obtained for 37 years (1980–2016) from the Global Flood Awareness System (GloFAS) dataset [38]. The streamflow data of each reservoir were then synthetically expanded to yield the daily time series for 1000 years. The top panels of Fig. 4 compare the historical observed records to the generated synthetic time series. The streamflow data shown (top left panel) are the aggregated total across the six reservoirs for each year. Note that the median of both records is similar in pattern and scale, while the envelope of the synthetic data extends beyond that of the historical record. This allows us to explore plausible inflow conditions outside of recent observed data.

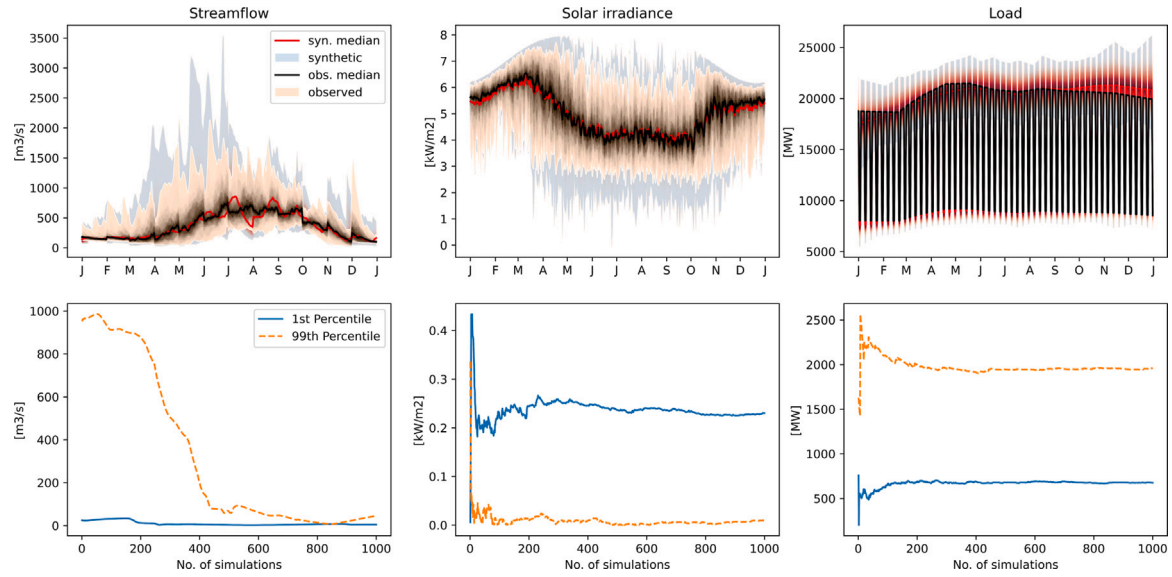

Fig. 4. Comparison of historical observed record and the 1000-year synthetic dataset of daily streamflow, solar irradiance and load (top panel). Absolute difference between the historical and simulated inputs in terms of their 1st and 99th percentile values, tracked as a function of the number of simulations (bottom panel).

3.2.2. Solar power

As we shall see in Section 3.3, our experimental setup includes a few scenarios where solar plants are integrated in the Cambodian grid. As solar power is non-dispatchable, the required input to PowNet are the hourly time series of solar availability. Solar power production is derived from solar irradiance using the GSEE package [39], which takes as input time series of solar irradiance, the coordinates of the solar plants, and the plant specifications (e.g., installed capacity, tilt angle). The hourly solar irradiance data for Cambodia were obtained for 39 years (1981–2019) from Renewables.ninja [40].

To generate the synthetic data, we model the deviations of observed irradiance from "clear sky" (cloudless) conditions, a method also used in [21,41]. We begin by identifying the 365-day "clear sky" profile and subtracting the observed irradiance for each calendar day to find the "losses" due to cloud cover:

$$I_d^l = I_{cs}^n - I_{obs}^d, \tag{5}$$

where I_d^l represents the irradiance "losses" on day d, I_{cs}^n the "clear sky' irradiance on calendar day n, and I_{obs}^d the observed irradiance on day d. The irradiance "losses" are then standardized to approximate a Gaussian distribution:

$$\widehat{I_d^l} = \frac{I_d^l - \mu(I_n^l)}{\sigma(I_n^l)}, \tag{6}$$

where $\widehat{I_d^l}$ is the standardized irradiance loss on day d, and $\mu(I_n^l)$ and $\sigma(I_n^l)$ are the average and standard deviation of I_d^l on calendar day n, respectively. We then model the resulting $\widehat{I_d^l}$ as an AutoRegressive Moving Average (ARMA) process with order (n_a, n_c):

$$\widehat{I_d^l} = \sum_{i=1}^{n_a} a_i I_{d-i}^l + \sum_{i=1}^{n_c} c_i \epsilon_{d-i} + \epsilon_d, \tag{7}$$

where a_i and c_i are the autoregressive and moving average coefficients, and $\epsilon_d \sim \mathcal{N}(0, \sigma^2)$ the error generated by a white Gaussian stochastic process. ARMA(2, 2) was selected to model the standardized irradiance losses as it resulted in the lowest Akaike Information Criterion (AIC) value (details of the ARMA model results can be found in Figure S3 in the SI). We then synthetically generate 1000 years of $\widehat{I_d^l}$ by first generating random values of ϵ_d and then propagating them through the ARMA model. The new time series of irradiance losses are obtained by reversing Eq. (6):

$$I_d^{l,new} = \widehat{I_d^l} \times \sigma(I_n^l) + \mu(I_n^l), \tag{8}$$

and the time series of solar irradiance are obtained by subtracting the losses from the clear sky profile,

$$I_d^{new} = I_{cs}^n - I_d^{l,new}. \tag{9}$$

As shown in Fig. 4 (top central panel), the synthetic solar irradiance has an envelope of variability going above and below the observed ones, representing conditions where we get varying amounts of solar.

3.2.3. Load

As mentioned in Section 2.3, the objective of PowNet is to meet the electricity demand at all substations at minimum cost. The hourly scheduling of power plants (including hydroelectric dams) is thus constrained by available supply, but also strongly driven by demand. This makes it important to explore the coupled system's responses under different load conditions. Since the only available time series of load data from technical reports in Cambodia are the monthly peak national demand data [32], these form the basis of our synthetic data generation. In particular, we employed a two-step approach to model the peak demand. First, we identify the variable related to temperature that can best model the observed peak demand data in each month using a linear regression model (see Figure S4 in the SI for additional details). This modelling assumption is justified by the fact that air temperature is a notable driver in electricity demand variations [42,43]. Next, we stochastically model two processes of interest—(i) minimum air temperature and (ii) the residuals between the predicted and observed peak demand—before combining them to get synthetic time series of peak demand.

We obtained the monthly peak demand data from [32] for six years (2011–2016), and daily minimum and maximum temperature data from the Climate Forecast System Reanalysis (CFSR) dataset [44] for 42 years (1975–2016). After performing a correlation analysis between the normalized peak demand and multiple variables related to temperature (see Figure S4 for additional details) for the common available period (2011–2016), we found that the peak demand in Cambodia has the strongest correlation ($r = 0.65$) with the monthly mean of the minimum air temperature averaged across Cambodia (see Figure S5 in the SI). This yields the following linear model:

$$d_m^{pred} = a \times \bar{t}_{min,m} + c, \tag{10}$$

where d_m^{pred} is the predicted peak demand in month m, $\bar{t}_{min,m}$ the mean of the daily minimum temperature in month m, and a and b the

coefficients of the linear regression model. The difference between the observed and fitted peak demand is $D_m = d_m^{obs} - d_m^{pred}$, where D_m is the time series of monthly difference, and d_m^{obs} the observed peak demand. We then model two variables stochastically (i) the daily minimum air temperature averaged across Cambodia, time series of which are then translated to monthly mean values for use in the peak demand model, and (ii) the stochastic difference between the predicted and actual peak demand D_m. Similar to the process used for solar irradiance, we standardize the two variables using Eqs. (11) and (12) respectively:

$$\hat{t}_{min,d} = \frac{t_{min,d} - \mu(t_{min,n})}{\sigma(t_{min,n})}, \tag{11}$$

$$\hat{D}_m = \frac{D_m - \mu(D_p)}{\sigma(D_p)}, \tag{12}$$

where $\hat{t}_{min,d}$ and $\hat{D}_m$ are the standardized temperature on day d and residual between the predicted and actual peak demand in month m, respectively. $t_{min,d}$ denotes the daily observed minimum temperature, and $\mu(t_{min,n})$ and $\sigma(t_{min,n})$ are its mean and standard deviation on calendar day n, while $\mu(D_p)$ and $\sigma(D_p)$ are the mean and standard deviation of D_m for each calendar month p. In the next step, we model $\hat{t}_{min,d}$ and $\hat{D}_m$ as separate ARMA processes, then synthetically generate 1000 years of time series for each of them (details of the ARMA model results can be found in Figure S6 in the SI). With the regression model found in Eq. (10), we then translate these 1000-year ensembles to synthetic time series of monthly peak demand d_m^{syn},

$$d_m^{syn} = a \times \bar{t}_{min,m}^{syn} + c + D_m^{syn}, \tag{13}$$

where $\bar{t}_{min,m}^{syn}$ is the mean of the synthetic minimum temperature in month m, and D_m^{syn} the synthetic errors between the predicted and actual peak demand in month m. The peak demand data are then transformed to hourly load at each substation following the method described in Section 3.1.

Fig. 4 (top right panel) shows the variation in the daily national load. The profile shows prominent rise and falls indicating the weekdays and weekends, and also has a synthetic envelope that allows us to explore the response of the system in conditions with high and low loads.

3.3. Experimental setup

Recall that the goal of our study is to understand the benefits of hard-coupling water and power system models. Our experimental design explores the benefits of this integration under: (1) stationary hydro-meteorological uncertainty (Section 3.2); and (2) current and future grid infrastructure scenarios, including future additions of renewable energy.

As Cambodia strives to both expand and decarbonize its grid, multiple solar farms are planned to be built for fulfilling the electricity demand up until 2030 [31]. We thus explore the addition of two solar nodes, one at Kampong Chhnang and another at Kampong Speu province, both near the capital Phnom Penh (Fig. 3). We model three different infrastructure configurations: (1) the 2016 as-is grid (400 MW coal, 282 MW oil, 1048 MW hydropower, and 320 MW imports), (2) the grid with 300 MW of solar capacity installed (two plants with 140 MW and 160 MW capacity), and (3) the grid with 600 MW of solar installed (two plants with 280 MW and 320 MW capacity). The location of the solar plants is based on the aforementioned reports, while the plant capacities are loosely based on the amount expected to be installed in the coming decade (so as to model the system under a broad range of conditions). These three grid configurations are referred to throughout the rest of this paper as Case 1, Case 2, and Case 3, respectively. Each grid configuration is simulated under two modelling implementations: (1) with hard-coupling of the water-energy models; and (2) without hard-coupling. The three grid configurations paired with hard-coupling of the water-energy models are referred to as Case 1H, Case 2H, and Case 3H, respectively. To determine the volume of simulations that should be conducted, we track the convergence between the 1st and 99th percentile values of the historical and synthetic inputs. As shown in Fig. 4 (bottom panel), we require at least 900, 300, and 200 simulations for streamflow, solar irradiance, and load, respectively, to achieve a stabilized distribution. In our study, we thus conducted our experiments with 1000 simulation years. Thus, our total number of simulated years is 6000 (1000 synthetic weather years x 3 grid configurations x 2 modelling implementations). In our study, we defined the convergence limit $\epsilon = 10^{-4}$, and maximum number of iterations $n = 10$. Typically, the re-operation model takes up to three iterations to calculate the updated release of the reservoir. The runtime (minutes) of each year of simulation with respect to different external drivers is reported in Figure S7. Based on simulations ran on an Intel(R) Core (TM) i7-8700 CPU 3.2 GHz with 8 GB RAM running Windows 10, the runtime varies between 20 and 65 min for the scenarios without feedback (Cases 1, 2 and 3). The addition of the feedback mechanism causes a larger range in computation time (up to two times) across the scenarios. In general, cases with a larger reservoir inflow and smaller load are more computationally demanding. Depending on the experimental set-up and simulation–optimization environment, each year of simulation on the Cambodian grid can take up to two hours.

4. Results

First, we report results from our probabilistic assessment of the benefits provided by the hard-coupled framework (Section 4.1). Then, we identify the key factors that affect such benefits, so as to understand their relevance in a real-world context (Section 4.2). Finally, we explore the effects of the hard coupling mechanism on the re-operation of individual grid components (Section 4.3).

4.1. System response to co-simulation

To quantify the potential benefits of the co-simulation framework, we consider three metrics, namely annual operating costs, CO_2 emissions, and penetration of renewables in the generation mix. Fig. 5 (top panel) illustrates the effects of hard coupling for each grid configuration aggregated across the 1000 synthetic weather years. The first key result to notice is that the adoption of the hard-coupling nearly always increases the penetration of variable renewable energy (wind and solar) and decreases both annual operating costs and CO_2 emissions, indicating that the benefits of the co-simulation framework are robust with respect to stationary uncertainty in streamflow, solar irradiance, and load. Importantly, this finding is consistent across the three grid configurations (i.e., current grid, +300 MW, and +600 MW of solar capacity).

The second result worth discussing here is the magnitude of the benefits reaped by the hard-coupling. Starting with the existing grid (Case 1 and 1H), the cost savings from hard-coupling range between 4% and 40% per year, while the CO_2 reduction ranges between 4% and 50%, reflecting the benefits of the curbed reliance of fossil fuels and corresponding increased penetration of renewables (range between 1% and 20%). As hydropower is the only renewable resource in Case 1 and 1H, the results suggest that the system's performance can be improved just by re-operating the reservoir, even before additional renewable energy is added. Shifting our focus to Scenarios 2 and 3, the addition of solar resources results in a slight increase in the penetration of renewables caused by hard-coupling, leading to further reductions in operating costs and CO_2 emissions. It is interesting to note that although the cumulative distribution functions of change in renewable integration do not seem to vary much across the three grid setups, the disparity of their effects on cost and CO_2 emissions are more pronounced. For example, there is a 50% chance of hard-coupling improving the operating costs by at least 15% in Case 1H, a chance that

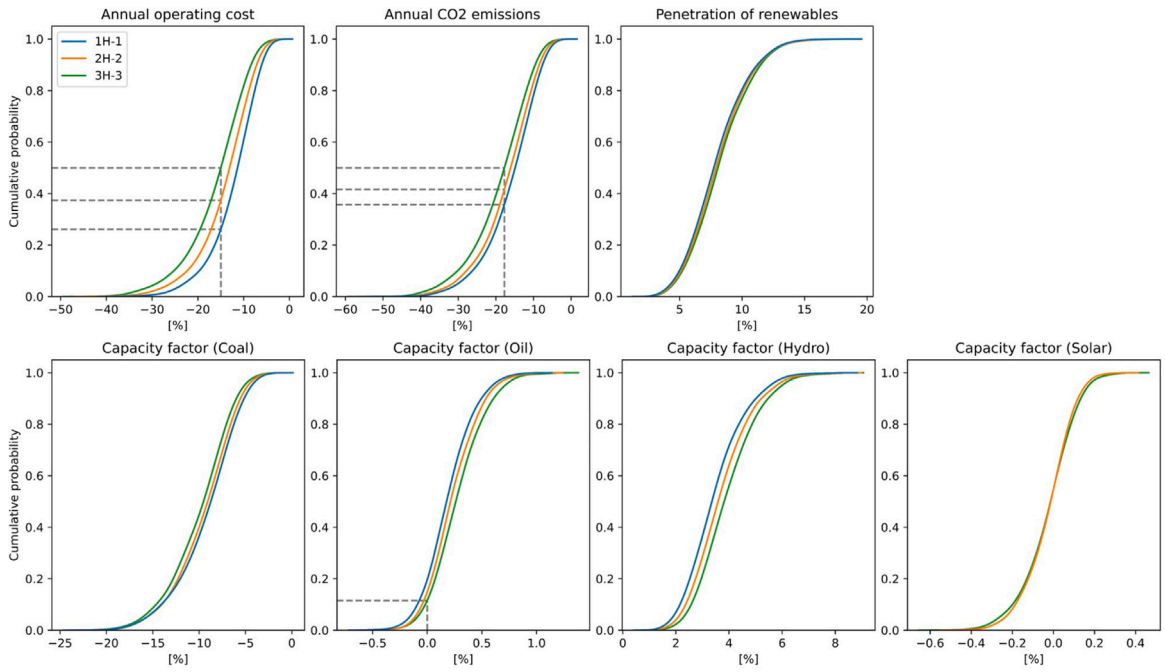

Fig. 5. Cumulative density plots illustrating the system's response, evaluated in terms of performance metrics (top panel) and plant capacity factors (bottom panel). The three lines in each plot represent the difference between the results obtained with and without hard coupling in the three infrastructure configurations. The system performance is measured in terms of annual operating cost, annual CO_2 emissions, and penetration of renewable in the generation mix. The plant capacity factors are calculated as a percentage of actual production in a year over the potential peak production of each generation type.

increases to 63% and 74% in Case 2H and 3H, respectively. A similar observation applies to CO_2 emissions.

We carry out a similar analysis for the capacity factor of the four generation types (i.e., coal, oil, hydropower, and solar), whose cumulative distribution functions are shown in Fig. 5 (bottom panel). This analysis reveals that different generation types exhibit different responses to the feedback mechanism added via model hard-coupling. For instance, the capacity factor of coal plants always decreases, while that of oil plants has a ~90% probability of increasing. Hydropower usage always increases (despite the same amount of water being available with and without hard-coupling). As we shall see in Section 4.3, the varying responses of the dispatchable power plants (coal, oil, hydropower) to the hard-coupling arise from factors such as plant locations and the reservoirs they are interconnected with. For example, two out of the three coal plants are directly connected to Kamchay, the reservoir with the biggest storage capacity (see Fig. 3 and Table 1). When the large reservoir is re-operated, the re-distribution of water resources increases the plant's hydropower production, reducing the capacity factor of the nearby coal plants by up to 25%. Conversely, the capacity factor of oil plants only varies between −0.5% and 1%. This can be attributed to their location, as most of them are near Phnom Penh (the main load-centre) and do not have direct interconnections with any hydropower reservoir.

4.2. Factors affecting performance of the feedback mechanism

Fig. 5 shows that the use of a hardly-coupled model always outperforms the benchmark modelling approach. It also shows that the magnitude of the benefits varies widely across years. It is therefore essential to understand how the hydro-meteorological conditions control the effectiveness of such hard integration. This is done through a parallel coordinate plot (Fig. 6), where we visualize the annual values of streamflow, load, and the system's response to the hard coupling obtained when moving from Case 1 to Case 1H. (similar analyses for Case 2/2H and 3/3H are reported in Figure S8 in the SI). The variables are shown across five parallel axes, so each line connecting the axes represents a single year of the 1000-year stochastic ensemble. Note that this analysis focuses on the ten years that result in the largest (99th percentile and above) and smallest (1st percentile and below) difference between the benchmark and hard-coupled formulations for operating costs and CO_2 emissions.

Fig. 6 illustrates three important behaviours. First, there is a strong correlation between costs and CO_2 emissions (see the horizontal lines crossing the last two axes), so the ranking of the simulation years does not change depending on which benefit we consider. This behaviour is easily explained by the fact that coal and oil plants have the highest operating costs and CO_2 emissions. Second, both total annual streamflow and load appear to control the extent of the benefits. Beginning with streamflow, it is intuitive that larger benefits will be reaped if the system has additional flexibility in storing water for more timely hydropower generation. If dams are better able to coordinate their release decisions with the state of the power grid, it follows that the grid should be able to rely less on fossil fuel power plants. This is evident in the "Annual available Q" axis, where the maximum benefit case corresponds to large values of Q in the top panel—while the highlighted lines are clustered near the bottom of the axis in the bottom panel. In other words, having a larger volume of water in the system allows greater flexibility in the re-operation (as shown in the third axis), thus hydropower generation can be better scheduled or deferred to allow for the use of solar (see Figure S8)—an opportunity that does not exist during dry years. Likewise, the frequency of reservoir re-operation also depends on load. We observe that years with high annual streamflow and low load (leading to more frequent periods of low net demand) are associated with the largest benefits from model hard-coupling, allowing annual cost savings of up to 44% and CO_2 reduction of up to 53%. Conversely, in years with low Q and high load, the benefits of greater flexibility in re-allocating water are diminished, resulting in an annual cost and CO_2 reduction of about 4%. Third, a prominent difference between the top and bottom panels stands in the dispersion of the values associated to the highlighted years—in the bottom panel the ten highlighted lines tend to converge around similar values. A possible explanation for this behaviour exists in the distribution of the inflow process: high-streamflow years are less concentrated around a

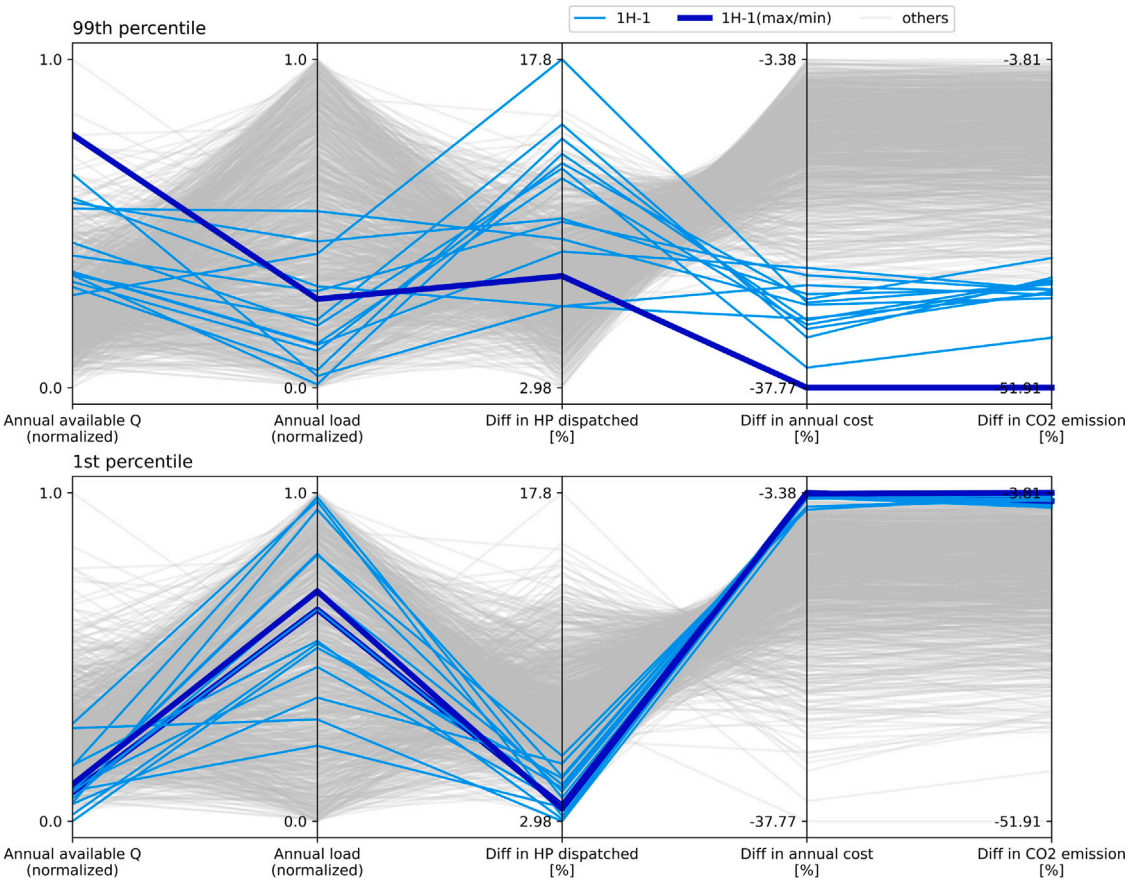

Fig. 6. Parallel coordinate plot illustrating the relation between input variables (streamflow (Q) and load) and the system's response to the hard coupling (annual hydropower dispatched, costs, and CO_2 emissions) obtained when moving from Case 1 to Case 1H. Each line corresponds to one of the 1000 simulation scenarios. In the top panel we highlight the years with the largest benefits (above the 99th percentile) in terms of the operating costs and CO_2 emissions, while in the bottom panel we highlight the years with the smallest benefit (below the 1st percentile). The bold lines represent the year with the maximum and minimum benefits, respectively, in the top and bottom panels. The analysis for Case 2/2H and 3/3H is reported in Figure S8 in the SI.

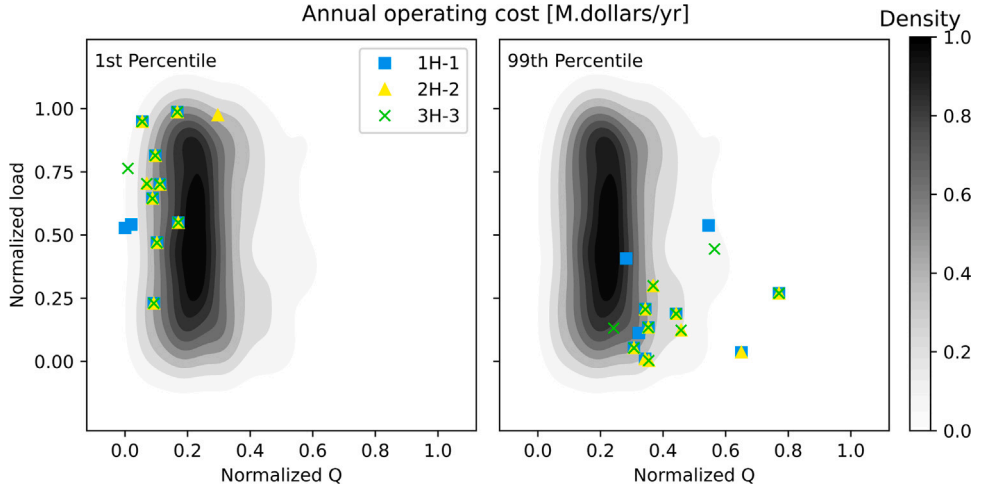

Fig. 7. Probabilistic assessment of the annual operating costs as a function of annual values of streamflow (Q, horizontal axis) and load (vertical axis). Their bivariate distribution (estimated with a Gaussian kernel) is represented by the isolines inside the plot. Each symbol represents a year that led to the largest (99th percentile and above) and smallest (1st percentile and below) operating cost reductions. Squares, triangles, and crosses correspond to the three grid configurations.

single value, while low-streamflow years tend to cluster around similar minimum values.

Having identified annual streamflow and load as the key factors that influence the benefits of hard-coupling in a given year, we then evaluate this finding across the different grid set-ups. Fig. 7 illustrates the joint distribution of total annual streamflow and load (estimated with a Gaussian kernel), and highlights the 1st and 99th percentile years in terms of annual operating cost for all grid set-ups. A similar plot highlighting the performance in terms of CO_2 emissions can be found in the SI (Figure S9). A visual comparison between the two panels shows that the points tend to cluster in specific regions of the streamflow-load space—the ones with the least benefits mostly lie on

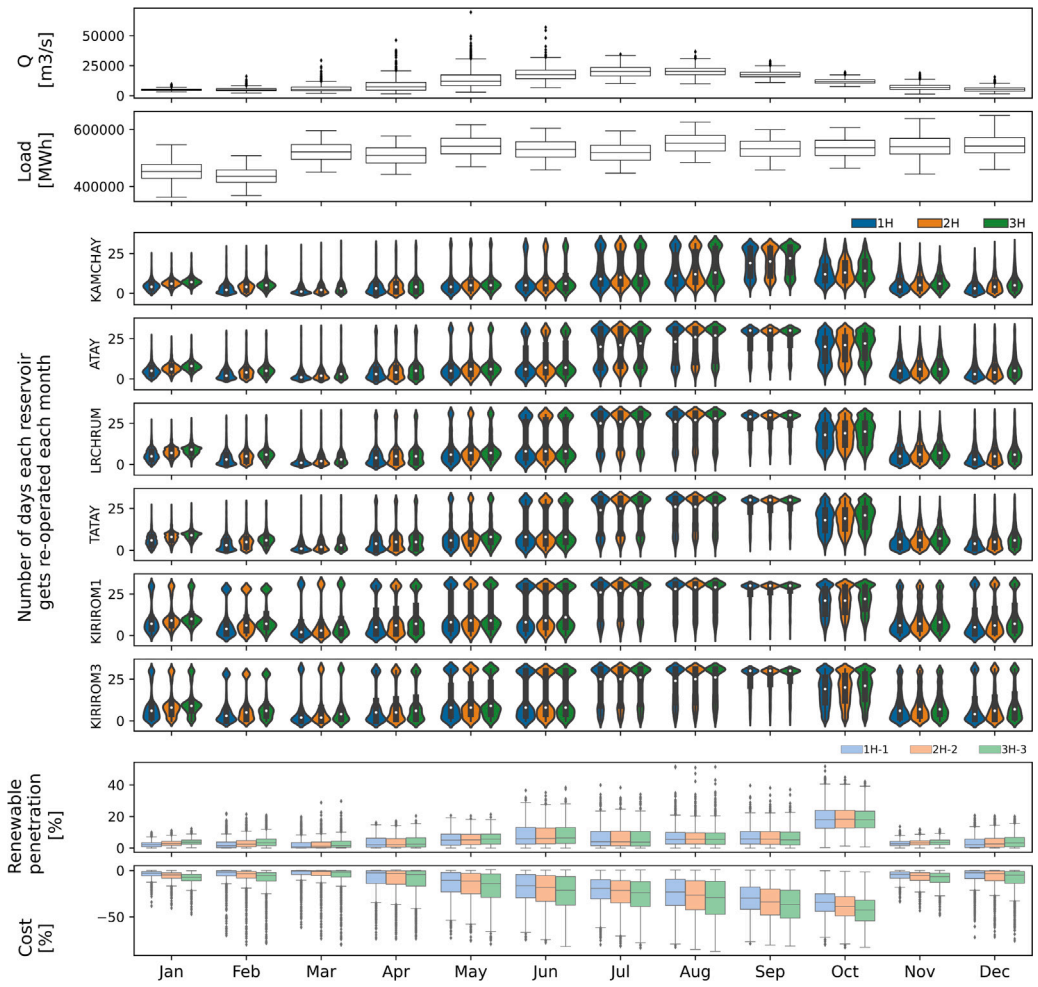

Fig. 8. Variability in input variables (streamflow (Q) and load), number of reservoir re-operations, and the resulting system's performance (increase in the penetration of renewables and decrease in operating costs) across different months.

the top left quadrant (small inflow, large load), while the ones with the largest benefits lie on the bottom right (large inflow, small load). This reinforces the finding that streamflow and load are the main factors that determine the effectiveness of the feedback mechanism in a given weather year.

4.3. Spatial and temporal effects of the feedback mechanism

With an understanding of how the external conditions influence the overall system's performance, we now explore how the re-operation mechanism modifies the grid behaviour at a finer spatio-temporal scale. This is achieved through an assessment of the month-to-month variability in the re-operation frequency for each hydropower reservoir, illustrated in Fig. 8 (central panels). By looking at the temporal patterns revealed by the violin plots, it is evident that the re-operation mechanism is heavily influenced by the seasonality of the monsoon (see the monthly total streamflow illustrated in Fig. 8, upper panel). For all six reservoirs, the number of days in which the re-operation is adopted is fairly modest in the pre-monsoon season (January to April), gradually increasing during the summer monsoon (May to October) and then decreasing in November–December. This pattern is a direct consequence of the control that water availability exerts on the benefits of the re-operation mechanism (Section 4.2). The violin plots also suggest that the monthly number of re-operations is rather stable during the central part of the monsoon season (i.e., July to September), while it tends to vary at the beginning and end—a result explained by the inter-annual variability in the monsoon season onset, withdrawal, and length [45].

The temporal patterns of the re-operation mechanism are reflected in the monthly operating costs and penetration of renewables (Fig. 8, bottom panels), which improve as the monsoon season unfolds. The best values for both metrics are observed in October, when the streamflow starts to decrease, a behaviour attributable to the use of water accumulated during the summer monsoon. As for the three grid configurations (Case 1, 2, and 3), the temporal patterns of reservoir re-operation are similar, although a closer inspection reveals that the reservoirs get increasingly re-operated with a larger capacity of solar in the system. With the addition of solar, the system is given the option to use an alternative non-dispatchable resource, causing a more frequent mismatch between the available and dispatched hydropower. Naturally, the deployment of more solar (Case 2/2H and 3/3H) further impacts the monthly operating costs and penetration of renewables.

Among the six reservoirs in the grid, Kamchay is re-operated the least. Spatially, the reservoirs can be divided into three main clusters, based on the interconnections of the transmission lines (refer to Fig. 3): (i) Atay, LR Chrum and Tatay, (ii) Kirirom I and Kirirom III, and (iii) Kamchay. The re-operation patterns exhibited by the reservoirs in groups (i) and (ii) are similar and well-reflected in the transmission line usage. Indeed, the increase in re-operation during the monsoon keeps the line usage within a narrow operational band (refer to Figure S10 in the SI). Since both clusters consist of multiple reservoirs grouped together, the power supply within each respective sub-grid comes primarily from hydropower, resulting in a very similar pattern between

re-operation and line usage. In contrast, Kamchay is a generating unit in a sub-grid that consists of other generating units, demand nodes, and transmission lines, all feeding Phnom Penh. The difference in response can be attributed to the complex interactions between the different components in the sub-grid. As seen in Section 4.1, different generators respond differently with the addition of the feedback mechanism. The hard coupling also influence the frequency of the N-1 violations (instances in which any of the high-voltage lines reaches 75% of its capacity) for the most congested lines (see Figure S10 in the SI). Taking the spatial and temporal variability together, the above analyses highlight that the topology of the grid, existing resources, and seasonal dynamics play a part in how the system responds to the hard-coupling. Given the role that hydropower reservoirs play in both systems, their operations have to be adapted to local conditions, an information that is not available in soft-coupling approaches.

5. Conclusions

Overall, our study contributes a novel modelling framework that co-simulates water and energy systems. The hard coupling is facilitated by a dam re-operation model able to handle both individual and multi-reservoir systems. By testing the coupled models under uncertainty in external conditions, we show robust improvements—w.r.t. a soft-coupling approach—in terms of system operating costs, CO_2 emissions, and penetration of renewables in the generation mix. This implies that through modelling the water and energy systems as a whole—instead of taking them as individual systems—more efficient operating patterns can be achieved. In particular, we show that the hard coupling works best in conditions of high water availability and low electricity demand, a condition that allows us to shift water volumes and hydropower production so as to 'optimally' track the intermittent production of other renewables. Because of this added flexibility, the benefits of co-simulation are expanded in cases with more solar deployed in the grid, where we see more renewable penetration in the generation mix (and more frequent periods of locational generation "oversupply"). Thus, our results suggest that co-simulation frameworks may be a useful tool to support not only operational decision-making, but also grid decarbonization efforts that are inevitably associated with major investment costs (e.g., Siala et al. [5] and Deshmukh et al. [46]). In this regard, it is worth stressing here that our results likely represent the upper bound of the benefits attainable through hard-coupling frameworks, because there might be unintended consequences of reservoir re-operations. For example, storing water during the monsoon season to track an increase of solar production may raise the frequency of spill events (see Figure S11 in the SI). Another potential consequence is hydropeaking, as a sudden surge in electricity demand may prompt operators to respond by releasing water from hydropower reservoirs, putting pressure on riverine ecosystems [47]. To address these potential challenges, knowledge about the behaviour of individual grid components—like the one revealed by our analysis—is therefore useful. For example, one could choose which dams to re-operate, where to place renewables, or whether to narrow the re-operation space.

Looking forward, we believe modelling frameworks like this one could potentially support many other research efforts in the water-energy domain. For example, seasonal streamflow forecasts are increasingly being used by hydropower operators to plan production schedules [48], so it is important to understand and quantify the relationship between forecast accuracy and value [49]—measured in monetary terms or added hydropower production. Such efforts may benefit of co-simulation environments, as they would help researchers account for all aspects (e.g., presence of other renewables, grid congestion problems) that are likely to affect the forecast value. Another example application in the hydropower industry domain are pumped hydro energy storage systems [50,51], whose operation is intrinsically connected to the state of the grid. Finally, research efforts should address the increase in computational requirements that is inevitably associated to the hard-coupling of water and energy models. If we find a solution to this issue, we then have a pathway to study the integration of renewables over larger spatial domains.

CRediT authorship contribution statement

Rachel Koh: Software, Methodology, Formal analysis, Investigation, Writing – original draft. **Jordan Kern:** Conceptualization, Methodology, Supervision, Writing – review & editing. **Stefano Galelli:** Conceptualization, Methodology, Visualization, Supervision, Writing – review & editing.

Declaration of competing interest

The authors declare that they have no known competing financial interests or personal relationships that could have appeared to influence the work reported in this paper.

Acknowledgement

Rachel Koh is supported by the President's Graduate Fellowship from the Singapore University of Technology and Design.

Appendix A. Supplementary data

Supplementary material related to this article can be found online at https://doi.org/10.1016/j.apenergy.2022.119386.

References

[1] Cabrera P, Carta J, Lund H, Thellufsen J. Large-scale optimal integration of wind and solar photovoltaic power in water-energy systems on islands. Energy Convers Manage 2021;235.
[2] Gonzalez J, Tomlinson J, Harou J, Ceseña E, Panteli M, Bottacin-Busolin A, Hurford A, Olivares M, Siddiqui A, Erfani T, Strzepek K. Spatial and sectoral benefit distribution in water-energy system design. Appl Energy 2020;269.
[3] Howells M, Hermann S, Welsch M, Bazilian M, Segerström R, Alfstad T, Gielen D, Rogner H, Fischer G, Van Velthuizen H, Wiberg D. Integrated analysis of climate change, land-use, energy and water strategies. Nature Clim Change 2013;3(7):621–6.
[4] Khan Z, Linares P, Rutten M, Parkinson S, Johnson N, García-González J. Spatial and temporal synchronization of water and energy systems: Towards a single integrated optimization model for long-term resource planning. Appl Energy 2018;210:499–517.
[5] Siala K, Chowdhury AK, Dang TD, Galelli S. Solar energy and regional coordination as a feasible alternative to large hydropower in southeast Asia. Nature Commun 2021;12(1):1–10.
[6] Zhou T, Voisin N, Fu T. Non-stationary hydropower generation projections constrained by environmental and electricity grid operations over the western united states. Environ Res Lett 2018;15(9).
[7] Kern JD, Su Y, Hill J. A retrospective study of the 2012–2016 California drought and its impacts on the power sector. Environ Res Lett 2020;15(9).
[8] Chowdhury AK, Dang TD, Nguyen H, Koh R, Galelli S. The greater Mekong's climate-water-energy nexus: How ENSO-triggered regional droughts affect power supply and CO_2 emissions. Earth's Future 2021;9(3).
[9] Francois B, Borga M, Creutin J-D, Hingray B, Raynaud D, Sauterleute J-F. Complementarity between solar and hydro power: Sensitivity study to climate characteristics in northern-Italy. Renew Energy 2016;86:543–53.
[10] Khan Z, Linares P, García-González J. Integrating water and energy models for policy driven applications. a review of contemporary work and recommendations for future developments. Renew Sustain Energy Rev 2017;67:1123–38.
[11] Voisin N, Kintner-Meyer M, Skaggs R, Nguyen T, Wu D, Dirks J, Xie Y, Hejazi M. Vulnerability of the US western electric grid to hydro-climatological conditions: How bad can it get? Energy 2016;115(1):1–12.
[12] Chowdhury AK, Kern J, Dang TD, Galelli S. PowNet: A network-constrained unit commitment/economic dispatch model for large-scale power systems analysis. J Open Res Softw 2020;8(1).
[13] Voisin N, Hamlet AF, Graham LP, Pierce DW, Barnett TP, Lettenmaier DP. The role of climate forecasts in western U.S. power planning. J Appl Meteorol Climatol 2006;45(5):653–73.
[14] Ibanez E, Magee T, Clement M, Brinkman G, Milligan M, Zagona E. Enhancing hydropower modeling in variable generation integration studies. Energy 2014;74:518–28.
[15] Stevanato N, Rocco M, Giuliani M, Castelletti A, Colombo E. Advancing the representation of reservoir hydropower in energy systems modelling: The case of Zambesi river basin. PLoS One 2021;16(12).
[16] Gebretsadik Y, Fant C, Strzepek K, Arndt C. Optimized reservoir operation model of regional wind and hydro power integration case study: Zambezi basin and South Africa. Appl Energy 2016;161:574–82.

[17] Sharpe E. West Texas needs electricity: The congested transmission problem. 2019, Energy Central, URL: https://www.energycentral.com/c/tr/west-texas-needs-electricity-congested-transmission-problem (last accessed on 11/12/2019).
[18] Chowdhury AK, Dang TD, Bagchi A, Galelli S. Expected benefits of Laos' hydropower development curbed by hydroclimatic variability and limited transmission capacity: Opportunities to reform. J Water Resour Plan Manage 2020;146(10):05020019.
[19] François B, Hingray B, Raynaud D, Borga M, Creutin J. Increasing climate-related-energy penetration by integrating run-of-the river hydropower to wind/solar mix. Renew Energy 2016;87:686–96.
[20] Zhang Y, Cheng C, Cai H, Jin X, Jia Z, Wu X, Su H, Yang T. Long-term stochastic model predictive control and efficiency assessment for hydro-wind-solar renewable energy supply system. Appl Energy 2022;316:119134.
[21] Su Y, Kern JD, Denaro S, Hill J, Reed P, Sun Y, Cohen J, Characklis GW. An open source model for quantifying risks in bulk electric power systems from spatially and temporally correlated hydrometeorological processes. Environ Model Softw 2020;126.
[22] Zagona EA, Fulp TJ, Shane R, Magee T, Goranflo HM. Riverware: A generalized tool for complex reservoir system modeling 1. JAWRA J Am Water Resour Assoc 2001;37(4):913–29.
[23] Labadie JW. MODSIM: Decision support system for integrated river basin management. In: Proceedings of the 3rd international congress on environmental modelling and software; 2006.
[24] Dang TD, Vu DT, Chowdhury AK, Galelli S. A software package for the representation and optimization of water reservoir operations in the VIC hydrologic model. Environ Model Softw 2020;126.
[25] Thurber TB, Vernon CR, Sun N, Turner SW, Yoon JJ, Voisin N. mosartwmpy: A python implementation of the MOSART-WM coupled hydrologic routing and water management model. J Open Source Softw 2021;6.
[26] Soncini-Sessa R, Weber E, Castelletti A. Integrated and participatory water resources management-theory. Amsterdam, The Netherlands: Elsevier; 2007.
[27] Vu DT, Dang TD, Galelli S, Hossain F. Satellite observations reveal thirteen years of reservoir filling strategies, operating rules, and hydrological alterations in the upper mekong river basin. Hydrol Earth Syst Sci Discuss 2021;1–28. http://dx.doi.org/10.5194/hess-2021-360.
[28] Pastor AV, Ludwig F, Biemans H, Hoff H, Kabat P. Accounting for environmental flow requirements in global water assessments. Hydrol Earth Syst Sci 2014;18(12):5041–59.
[29] Brown T, Hörsch J, Schlachtberger D. PyPSA: Python for power system analysis. J Open Res Softw 2018;6(1).
[30] Gomes C, Thule C, Broman D, Larsen PG, Vangheluwe H. Co-simulation: A survey. ACM Comput Surv 2018;51(3):1–33.
[31] EDC. Current state of Cambodia's electricity demands and supply outlook. URL: https://amchamcambodia.net/wp-content/uploads/2019/08/Outlook-of-demand-and-supply-1.pdf.
[32] EDC. Annual report 2016. Technical report, Electricité du Cambodge (EDC); 2016.
[33] JICA. Preparatory survey for Phnom Penh city transmission and distribution system expansion project phase II in the Kingdom of Cambodia. Technical report, Japan International Cooperation Agency (JICA); 2014.
[34] Giuliani M, Herman J, Quinn J. Kirsch nowak streamflow generator. 2016, https://https://github.com/julianneq/Kirsch-Nowak_Streamflow_Generator.
[35] Quinn JD, Reed PM, Giuliani M, Castelletti A, Oyler JW, Nicholas RE. Exploring how changing monsoonal dynamics and human pressures challenge multireservoir management for flood protection, hydropower production, and agricultural water supply. Water Resour Res 2018;54(7):4638–62.
[36] Giuliani M, Quinn J, Herman J, Castelletti A, Reed P. Scalable multiobjective control for large-scale water resources systems under uncertainty. IEEE Trans Control Syst Technol 2017;26(4):1492–9.
[37] Quinn J, Reed P, Giuliani M, Castelletti A. Rival framings: A framework for discovering how problem formulation uncertainties shape risk management trade-offs in water resources systems. Water Resour Res 2017;53(8):7208–33.
[38] Harrigan S, Zsoter E, Barnard C, F. W, Salamon P, Prudhomme C. River discharge and related historical data from the global flood awareness system, v2.1, copernicus climate change service (C3S) climate data store (CDS). 2019, URL: https://doi.org/10.24381/cds.a4fdd6b9.
[39] Pfenninger S, Staffell I. Long-term patterns of European PV output using 30 years of validated hourly reanalysis and satellite data. Energy 2016;114:1251–65.
[40] Gelaro R, McCarty W, Suárez M, Todling R, Molod A, Takacs L, Randles C, Darmenov A, Bosilovich MG, Reichle R, Wargan K. The modern-era retrospective analysis for research and applications, version 2 (MERRA-2). J Clim 2017;30(14):5419–54.
[41] Su Y, Kern JD, Reed P, Characklis GW. Compound hydrometeorological extremes across multiple timescales drive volatility in California electricity market prices and emissions. Appl Energy 2020;276.
[42] Apadula F, Bassini A, Elli A, Scapin S. Relationships between meteorological variables and monthly electricity demand. Appl Energy 2012;98:346–56.
[43] Moral-Carcedo J, Vicéns-Otero J. Modelling the non-linear response of Spanish electricity demand to temperature variations. Energy Econ 2005;27(3):477–94.
[44] National Center for Atmospheric Research Staff (Eds). The climate data guide: Climate forecast system reanalysis (CFSR). URL: https://climatedataguide.ucar.edu/climate-data/climate-forecast-system-reanalysis-cfsr.
[45] Cook BI, Buckley BM. Objective determination of monsoon season onset, withdrawal, and length. J Geophys Res: Atmos 2009;114(D23).
[46] Deshmukh R, Phadke A, Callaway DS. Least-cost targets and avoided fossil fuel capacity in India's pursuit of renewable energy. Proc Natl Acad Sci 2021;118(13).
[47] Haghighi AT, Ashraf FB, Riml J, Koskela J, Klø ve B, Marttila H. A power market-based operation support model for sub-daily hydropower regulation practices. Appl Energy 2019;255:113905.
[48] Troin M, Arsenault R, Wood AW, Brissette F, Martel J-L. Generating ensemble streamflow forecasts: A review of methods and approaches over the past 40 years. Water Resour Res 2021;56(7):e2020WR028392.
[49] Turner SW, Bennett JC, Robertson DE, Galelli S. Complex relationship between seasonal streamflow forecast skill and value in reservoir operations. Hydrol Earth Syst Sci 2017;21(9):4841–59.
[50] Rehman S, Al-Hadhrami LM, Alam MM. Pumped hydro energy storage system: A technological review. Renew Sustain Energy Rev 2015;44:586–98.
[51] Kocaman AS, Modi V. Value of pumped hydro storage in a hybrid energy generation and allocation system. Appl Energy 2017;205:1202–15.